Dendrimer-modified Gold Nanorods as a Platform for Combinational Gene Therapy and Photothermal Therapy of Tumors

Lili Ye
Southern Medical University
Yaoming Chen
Zhujiang Hospital
Jizong Mao
Zhujiang Hospital
Xiaotian Lei
Zhujiang Hospital
Qian Yang
Zhujiang Hospital
chunhui cui (chunhuicui12@126.com)
Southern Medical University

Research Article

Keywords: dendrimers, gold nanorods, gene delivery, photothermal therapy, cancer treatment

Posted Date: March 16th, 2021

DOI: https://doi.org/10.21203/rs.3.rs-263824/v1

Abstract

Background: The exploitation of novel nanomaterials combining diagnostic and therapeutic functionalities within one single nanoplatform is challenging for tumor theranostics.

Methods: In this work, we synthesized dendrimer-modified gold nanorods for combinational gene therapy and photothermal therapy (PTT) of cancer cells. Seed-mediated synthesized gold nanorods were modified with GX1 peptide-modified amine-termi-nated generation 3 poly(amidoamine) dendrimers via Au-S bond. The obtained GX1 modified dendrimer-stabilized Au NRs (Au NR@PAMAM-GX1) are performed as a gene delivery vector to gene (FAM172A) for computed tomography (CT) imaging, thermal imaging, photothermal therapy (PTT) and gene therapy of Colon cancer cells (HCT-8 cells).

Results: We find that Au NR @ PAMAM-GX1 can specifically deliver FAM172A to cancer cells with excellent transfection efficiency. The HCT-8 cells treated with the Au NR@PAMAM-GX1/FAM172A under laser irradiation have a viability of 20.45%, which is much lower than the survival rate of other single-mode PTT treatment or single-mode gene therapy. In addition, animal experiment results confirm that Au NR@PAMAM-GX1/FAM172A complexes can achieve tumor thermal imaging, PTT and gene therapy after tail vein injection.

Conclusion: The synthesized Au NR@PAMAM-GX1 is a potential nanoplatform for tumor imaging and treatment.

Background

Traditional cancer treatments such as surgery, chemotherapy and radiotherapy have serious flaws. For example, when tumor cells infiltrate the surrounding tissues or organs or adhere to the surrounding blood vessels and important organs, forced resection can be life-threatening; long-term chemotherapy causes tumors to develop resistance to many drugs, making cancer treatment difficult; besides, using the same method to kill cancer cells may also cause damage to healthy tissues or organs, causing side effects, including insomnia, vomiting, loss of appetite, and leukopenia. (1, 2)Therefore, it is important to develop a multifunctional nano-platform that combines different treatment methods such as genes treatment, drug therapy, photodynamic therapy and photothermal therapy (PTT).

In recent years, PTT has been regarded as an effective method for treating cancer because of its low cost, good local tumor treatment effect, and minimal side effects.(3–5) PTT can produce a significant cytotoxic effect on tumor tissue by generating hyperthermia, that is, the absorbed light is converted into local heat. For photothermal therapy of tumors, different nanomaterials platforms have been designed including carbon nanotubes,(6) graphene oxide,(7) and gold nanoparticles with different shapes (nanorods(8), nanostars(9), Au nano matryoshkas, nanochains(10)), Fe_3O_4 nanoparticles(11). Although these nanoplatforms have improved the therapeutic performance, some of them have complex and time-consuming synthesis processes. Therefore, the development of simple and multifunctional nano-

platforms as nanocarriers, photothermal agents and imaging agents is of great significance for collaborative phototherapy.

Gold nanorods (Au NRs) are one of the more popular nanomaterials because of their excellent physical and chemical properties such as simple preparation, surface functionalization, low toxicity, good biocompatibility and rich biological activity.(12–14) They have been widely studied and used as a nano-delivery nanoplatform for multimodal tumor therapy, such as drug therapy(15), photodynamic therapy (16)and gene delivery(17). In particular, GNRs have different surface plasmon resonance (SPR) enhanced absorption bands in the near-infrared spectral region by adjusting the size and aspect ratio (aspect ratio) of GNRs(18). Therefore, gold nanorods are considered as attractive candidates for photothermal therapy (PTT) because blood and soft tissues have relatively low attenuation of light.

However, due to the limited penetration depth of PTT, it is not ideal for the treatment of tumors located deep(19). Gene therapy as an adjunct therapy can overcome this shortcoming. Gene therapy (GT) is a promising method. It can introduce specific genes into target cells, restore defective genes or promote specific cell functions, so as to achieve long-term treatment(20, 21). Wang successfully synthesized a heterogeneous nanostructure (quasar Au@SiO_2) with hollow nanostars with encapsulated gold caps. Using the unique photothermal properties of the gold nanocomposite and the cavity properties of silica nanostars, complementary PTT/GT/chemotherapy can be achieved. In addition, PA and CT imaging can achieve image-guided therapy. (22)In another work, Xu and colleagues synthesized a multifunctional pDNA-conjugated polycation gold nano-coating Fe_3O_4 layered nanocomposite for three-modality imaging and photothermal/gene therapy.(23) Overall, the studies indicate that it is necessary to develop a unique multi-functional nanoplatform, which can be used for imaging-guided tumor combination therapy.

In this work, we developed a simple method to synthesize dendrimer-modified gold nanorods for combining gene silencing and tumor PTT (Scheme 1). First, gold nanorods were synthesized by the seed-mediated template method. Through the Au-S bond, partially thiolated third-generation (G3) poly (amidoamine) (PAMAM) dendrimers were combined with gold nanorods to form Au NR@PAMAM conjugate. Subsequently, GX1 Peptide was coupled by 1-ethyl-3- [3-dimethylaminopropyl] carbodiimide hydrochloride (EDC) coupling chemistry Modified onto the particle surface. The thus formed GX1-modified dendrimer-stabilized Au NR (Au NR @ PAMAM-GX1) serves as a carrier and loads DNA through electrostatic interaction. The obtained Au NR @ PAMAM-GX1/FAM172A complex was comprehensively characterized in terms of structure, composition, size, shape, surface potential, CT imaging and so on. The results of in vitro cell experiments showed that Au NR@PAMAM-GX1/siRNA complex has good cell compatibility and excellent gene transfection efficiency. In vivo anti-tumor studies have shown that the combination of photothermal and gene therapy is the best.

Methods

Materials

All chemical reagents were bought from commercial suppliers and used without further purification. Cetyltrimethylammonium bromide (CTAB), chloroauric acid ($HAuCl_4$), sodium borohydride ($NaBH_4$), silver nitrate ($AgNO_3$), L-ascorbic acid, methyl 2-sulfanylacetate, ethylenediamine and methyl acrylate were obtained from Aladdin (Shanghai, China). N-hydroxysuccinimide (NHS), 1-(3-dimethylaminopropyl)-3-ethylcarbodiimide (EDC). GX1 peptide was bought from Chu Peptide Biotechnology Co., Ltd (Shanghai, China). FAM172A were from Ruibo Biological Technology Co., Ltd (Guangzhou, China).

Synthesis of PAMAM-G_3

PAMAM dendrimers were synthesized using the divergence method. (24) Briefly, an appropriate amount of methanol was added to a three-necked flask with a magnetic stirrer, a reflux condenser, and a thermometer. Ethylenediamine was dissolved in anhydrous methanol and added dropwise to an excessive amount of methyl acrylate in methanol solution while continuously stirring for 48 hours, and then the solvent and monomer were distilled off under reduced pressure to obtain PAMAM-G0.5 dendrimer. The PAMAM-$G_{0.5}$ dendrimer was dissolved in anhydrous methanol, and then added dropwise to an excess of ethylenediamine in methanol solution with a drop rate of 1 drop/second while continuously stirring for 48 hours. The methanol and excess ethylenediamine were distilled off under reduced pressure to obtain a PAMAM-$G_{1.0}$ dendrimer. PAMAM-$G_{3.0}$ was obtained by repeating the above reactions twice.

Synthesis of Au NR

GNRs with long-wavelength LSPR peaks at 800 nm were synthesized in an aqueous solution using the seed-mediated template-assisted protocol.(25) Briefly, 0.6 mL of 10 mM ice-cold $NaBH_4$ was injected into a 10 mL aqueous solution containing 0.1 M CTAB and 0.25 mM $HAuCl_4$, under vigorous stirring. 0.2 mL of 25 M $HAuCl_4$ was added to 10 mL of 0.1 M CTAB to prepare the GNR growth solution. Then, 40 μL of 16 mM $AgNO_3$ and 90 μL 80 mM ascorbic acid were respectively added to the solution. After shaking, the growth liquid became colorless, and 12 μL of the previously prepared gold seed solution was injected therein. The solution was allowed to stand at 37°C for 12 hours to promote GNRs growth. The synthesized GNRs were purified by centrifugation twice at 8000 rpm for 10 min, and then re-dispersed in deionized water.

Synthesis of Au NR@PAMAM

According to reports in the literature, a partially thiolated G_3 (G_3-SH) was synthesized.(26) After that, under ultrasonic treatment, the aqueous solution of G_3-SH (20 mg in 1 mL of water) and Au NSs (10 mL) were mixed for 15 minutes, and then stirred at room temperature for another 24 h. The purified Au NR@PAMAM were obtained by centrifugation three at 8000 rpm for 10 min and dispersed in DI water.

Synthesis of Au NR@PAMAM-GX1

1.6 molar equivalents of EDC and NHS were added to 1 mL of GX1 (20 mg / mL, DMSO) solution and stirred for 4 hours. Then, the above solution was added to the Au NR@PAMAM dispersion and mix under continuous stirring overnight. Finally, The purified Au NR@PAMAM-GX1 were obtained by centrifugation three at 8000 rpm for 10 min and resuspended in DI water.

Characterization

The chemical structures of PAMAM and PAMAM-SH was confirmed by ^{1}H NMR spectroscopy (300 MHz, Varian, USA) with deuterium oxide (D_2O) as the solvent. The morphology of Au NR@CTAB was observed using transmission electron microscopy (JEOL TEM-1210) at 120 kV. Zeta potential and particle size were measured with a Nano-ZS instrument (Malvern Instru-ments Limited, England). UV-Vis spectra of PAMAM-SH, Au NR@CTBA, and Au NR@PAMAM were examined on a UV-2450/2250 (Shimadzu) spectrophotometer with the wavelength ranging from 200 nm to 900 nm. The Fourier transform infrared (FTIR) spectra of all samples were recorded in a Nexus 670 FT-IR spectrophotometer (Nicolet) in transmission mode with a KBr plate. The components of Au NR@PAMAM and AuNR@PAMAM-GX1 were determined using thermogravimetric analysis (Shimadzu TGA-50).

Preparation of Au NR@PAMAM-GX1/pDNA complex

To obtain Au NR@PAMAM-GX1/pDNA complexes, Appropriate amount of pDNA was added to the Au NR@PAMAM-GX1 solutions. Then, the mixture was incubated at room temperature for 30 min to form Au NR@PAMAM-GX1/pDNA complexes.

Agarose gel retardation assay

The pDNA condensing ability of Au NR@PAMAM-GX1 was examined by agarose gel retardation electrophoresis assay. In short, the AuNR@PAMAM-GX1/pDNA complexes with different N/P ratios were separated by 1% agarose gel electrophoresis containing Gold View II (Sigma) at 150 V for 15 minutes. After that, a gel imaging analysis system (Bio-Rad, Bio-Doc-ITM, USA) was used to capture images.

Complex Size and Potential

The hydrodynamic sizes and zeta potentials of Au NR@PAMAM-GX1/pDNA complexes were assessed at room temperature using a Malvern Zetasizer Nano ZS system. Data were recorded through three independent experiments.

Cytotoxicity of Au NR@PAMAM-GX1

Cytotoxicity of Au NR@PAMAM-GX1 was tested on HCT-8 cells and L929 cells. Briefly, HCT-8 cells were seeded in 96-well plates at 1×10^4 cells in each well and incubated in a 37 °C humidified incubator (5% CO_2) for 12 h. Then, the cells were treated with fresh cell medium containing Au NR@PAMAM-GX1 with concentrations ranging from 10 to 100 μg/mL and incubated for 24 h. After that, cells were washed with PBS and added with fresh cell medium containing 10% CCK-8 to all wells. The cell viability was determined with a microplate reader (MultiskanMk3, USA) HCT-8 cells treated with RPMI 1640 medium were used as control. Cytotoxicity of AuNR@PAMAM-GX1 was tested on L929 cells by the same method.

Cellular uptake of Au NR@PAMAM-GX1 complex

The cellular uptake of Au NR@PAMAM-GX1 by HCT-8 cells was quantified using confocal laser scanning microscopy (CLSM) measurements. Before measurement, Au NR@PAMAM-GX1 was labeled by FITC showing green fluorescence. In detail, HCT-8 cells were seeded in a 2 cm confocal microscopy dish at a density of 2×10^5 cells per well and incubated for 12 h. Then, cells were treated with FITC-labeled Au NR@PAMAM-GX1 and incubated for a different time. After each interval 1 h, 3 h and 6 h), the cells were washed with PBS and stained with 4',6-diamidino-2-phenylindole (DAPI) for 10 min at 37 °C. Finally, the cells were washed again and incubated with 2 mL of PBS for further observation. The Fluorescent pictures were captured by CLSM. Note that nuclei were stained by DAPI displaying blue fluorescence.

GX1 targeting ability assay

Cellular uptake of Au NR@PAMAM-GX1 complex with and without GX1 functionalization was analyzed to confirm the targeting ability of GX1. In detail, HCT-8 cells were seeded in 24-well plate with a density of 5×10^4 cells/well and incubated in a 37 °C humidified incubator (5% CO_2) for 12 h. Then, FITC-labeled Au NR@PAMAM or Au NR@PAMAM-GX1 complex was added to treat the cells and incubated for a different time. After each interval (1 h, 3 h and 6 h), cells in each group were washed by PBS, trypsinized, centrifuged and resuspended in 200 μL PBS in an Eppendorf tube. Finally, samples were measured using flow cytometry and the corresponding fluorescent intensity was quantified by Flow Jo 7.6.1 software.

In vitro gene transfection assay

HCT-8 cells were seeded in a 24-well plate at a density of 5×10^4 per well and cultured overnight before transfection. Then, cells were replenished with fresh media containing Au NR@PAMAM-GX1/pDNA complexes with different ratios (N/P ratio =15,20,30,40 and 50). After 24h incubation, the cells were tested for green fluorescent protein (GFP) expression with a fluorescence microscope (Zeiss, German). Then, cells were digested by trypsinized and resuspended in 0.5 μL PBS solution. the transfection efficiency was recorded using flow cytometry (BD Accuri C6). In this experiment, the cells were treated

with PBS and Au NR@PAMAM-GX1 were set as the negative control, where PEI-25k/pDNA was used as the positive control.

PTT and gene therapy in vitro

We first studied the potential of Au NR@PAMAM-GX1 to ablate cancer cells by photothermal ablation *in vitro*. Briefly, HCT-8 cells were sown in 96-well plates at a density of 1×10^4 cells/100 μL DMEM and cultured at 37 °C with 5% carbon dioxide overnight. After incubated with Au NR@PAMAM-GX1 at different Au concentrations for 24 h, these cells were washed 3 times with PBS and treated with 100μL fresh medium, followed by irradiation with near-infrared laser (808 nm, 1 W/cm^2) for 5 minutes. Finally, the CCK-8 assay was used to evaluate cell viability.

In addition, we also used the CCK-8 method to explore the *in vitro* experiments of PTT combined with gene therapy for tumor cells. HCT-8 cells were seeded and cultured as described above, after treated with Au NR@PAMAM-GX1 or Au NR@PAMAM-GX1/FAM172A polyplexes (N/P = 40: 1, 1 μg DNA) for 24 h, the cells were washed 3 times with PBS and incubated with 100 μL FBS-free medium, followed by irradiation with near-infrared laser (808 nm, 1 W/cm^2) for 5 minutes. Finally, the CCK-8 method and Zeiss inverted fluorescence microscope were used to observe calmodulin am stained cells to evaluate cell viability.

Apoptosis assay

HCT-8 cells were seeded in a 24-well plate at a density of 5×10^4 cells/well and incubated overnight. Then the culture medium was renewed by RPMI 1640 medium containing Au NR@PAMAM-GX1 or Au NR@PAMAM-GX1/FAM172A complexes with N/P ratio of 40. After 6h incubation, the cells were irradiated with 808 nm laster (1 W/cm^2,5 min). Cells untreated and only treated with laser irradiation or Au NR@PAMAM-GX1 was tested as the control. After further incubation 18 h, cells were digested by trypsinized and resuspended in 200 μL binding buffer. Then, the cells were stained with 5 μL V-PE and 5 μL 7-AAD and incubated for 15 min in the dark at room temperature. Finally, the apoptotic cells were analyzed using flow cytometry.

CT image

X-ray attention property of Au NR@PAMAM-GX1 was performed using a GE LightSpeed VCT imaging system (GE Medical Systems, Milwaukee, WI). Each CT scan was captured at 100 kV, 80 mA and a slice thickness of 0.625 nm. Au NR@PAMAM-GX1 dispersion under series of Au concentration was prepared in 0.2 mL Eppendorf tubes and all tubes were placed in the CT imaging system for scanning. CT images were recorded and Hounsfield units (HU) were measured using the built-in software.

Photothermal property of the AuNR@PAMAM-GX1

The photothermal property and stability of the Au NR@PAMAM-GX1 were examined. The aqueous suspension of Au NR@PAMAM-GX1solution with different Au concentrations (10, 20 and 40 μg/mL) were added into a cuvette, followed by irradiating with an 808 nm NIR laser (Changchun Lei Rui Optoelectronics Technology Co., Ltd.) at a power density of 1.5 W/cm^2 for 300 s. The temperature of different samples was recorded using a thermocouple probe every 10 s. The photothermal images were of Au NR@PAMAM-GX1 were captured using an infrared thermal imaging camera (Fotric 226). Next, the Au NR@PAMAM-GX1 with an equivalent concentration of 40 μg/mL were exposed to irradiation with a NIR laser for 300 s, with the laser density set at 0.5, 1, 1.5and 2.0 W/cm^2. In addition, we tested the photothermal stability of Au NR@PAMAM-GX1 by illuminating the Au NR@PAMAM-GX1 aqueous solution (40 μg/mL) using an 808 nm laser for 300s (1.5W/cm^2), and the suspension was cooled down to room temperature for 300 s. The irradiation and cooling process was carried out four times.

In Vivo Infrared Thermal Imaging Studies

In vivo infrared thermal imaging was captured using an infrared thermal imaging camera. HCT-8 tumor-bearing nude mice were narcotized with trichloroacetaldehyde hydrate (4%, 0.1 mL/10g) first while maintaining normal vital signs.100 μL of Au NR@PAMAM or 100 μL of Au NR@PAMAM-GX1 or 100 μL of PBS was then injected into the tumor-bearing mice through tail intravenous injection. Six hours after injection, the mice were irradiated with laser (808 nm, 1 W/cm^2), and the thermal image of the mouse and the temperature distributions of the mouse body were recorded using an infrared thermal imager.

Tumor Inhibition Assay

HCT-8 tumor-bearing nude mice were randomly divided into five groups with 3 mice per group: PBS (injected with PBS), NIR (injected with PBS and irradiated by NIR laser), Au NR@PAMAM-GX1 ([Au] =0.5mg/kg), Au NR@PAMAM-GX1+NIR (injected with Au NR@PAMAM-GX1 and irradiated by NIR laser, [Au] = 0.5mg/kg), injected with Au NR@PAMAM-GX1/FAM172 (injected with injected with Au NR@PAMAM-GX1/FAM172, [Au] = 0.5mg/kg FAM172=10mg/kg), Au NR@PAMAM-GX1/FAM172+NIR, (injected with Au NR@PAMAM-GX1/FAM172 and irradiated by NIR laser, [Au] = 0.5mg/kg, FAM172=10mg/kg). Herein, the NIR means light irradiation by an 808 nm-laser at a power density of 1 W/cm^2 for 5 min. After the treatment, the size of the tumors was measured using an electronic caliper every two days. The volumes of the tumors were calculated as 1/2×shortest diameter^2×longest diameter. The weight of mice was recorded at the same time. After 14 days of feeding, the tumors were photographed and weighted.

Histologic and Immunohistochemical Analysis

The mice of all groups were killed after the treatment. The tumors were removed, embedded in paraffin, and cryosectioned into 4 μm slices. Then, the sections were stained with H & E. For immunohistochemical analysis, the level of tumor apoptosis was examined using the terminal deoxynucleotidyl transferase deoxyuridine triphosphate nick-end labeling (TUNEL) assay. In addition, the expression of Ki67 in tumor sections was also detected.

Statistical analysis

The data were expressed as the mean standard deviation or standard error. Student's t-test was used for comparison between groups, and analysis of variance was used for more than two groups. P value <0.05 was considered statistically significant.

Results

Synthesis and Characterization of the Au NR@PAMAM-GX1

CTAB-coated Au NRs were synthesized by a seed-mediated method. Partially thiolated G3 PAMAM dendrimers were obtained by reacting G3.0 PAMAM dendrimers with methyl mercapto acetate. The resultant Au NRs were conjugated with thiolated G3.0 dendrimers via Au-S bond formation. The Au NR@PAMAM-GX1 was prepared by GX1 with Au NR@PAMAM. The Au NR@PAMAM-GX1 was combined with the FAM172A for CT/thermos imaging and the combination of PTT and gene therapy of tumors.

The synthesis of G3-SH was first characterized by ^{1}H NMR spectroscopy (Figure1A). Compared with amine-terminated G3, G3-SH shows an additional peak at 3.40 ppm, which can be assigned to the characteristic methylene peak of -NHCO-CH_2-SH. CTAB-coated Au NRs with a mean diameter of 35.5 nm were first obtained according to the literature. Transmission electron microscopy (TEM) images (Figure S1) indicated that the formed Au NRs have a nice rod shape with the average length and width were ~50 and ~20 nm. The optical properties of Au NR @ PAMAM-GX1 was tested by UV-Vis spectroscopy (Figure 1B). Compared with Au NR@CTAB, which has obvious absorption characteristics in the near-infrared region, the formed Au NR@PAMAM-GX1 has a clear surface plasmon resonance (SPR) peak 720 nm, which shows the hugeness in PTT applications potential. Compared with Au NR@CTAB before dendrimer grafting, dendrimer plus GX1 peptide modification to Au NR does not seem to cause a significant SPR change. TG measurement quantified the composition of the Au NR@PAMAM-GX1, in which Au, PAMAM dendrites and GX1 accounted for 22.4% ,74.04% and 3.56% of the entire nanosystem, respectively (Figure 1C). We measured the hydrodynamic diameter (D_h) of the nanosystems. As shown in Figure 1D, Au NR@PAMAM and Au NR@PAMAM-GX1 have a narrower size distribution, with D_h of 74 nm and 102 nm, respectively. In addition, the GX1 combination slightly reduced the positive surface charge of Au NR@PAMAM (Figure 1E), but the total charge of Au NR@PAMAM-GX1 was still positive. As a biological material, its solubility and stability are essential conditions. FTIR measurement shows that GX1 is

functionalized, and it is found that the peptide has a typical disulfide bond absorption peak at a wavelength of 511 cm^{-1}(Figure 1F).

Photothermal Property of the Au NR@PAMAM-GX1

Due to gold nanorods have strong tunable absorption in the near-infrared spectrum region, their photothermal effects have been widely studied and applied in photothermal therapy in vivo and in vivo. We measured the photothermal property of the Au NR@PAMAM-GX1 using an 808 nm laser. The photothermal heating curve tested by the infrared thermal camera showed strong concentration-dependent effects (Figure 2A and 2B) and laser power-dependent effects (Figure 2C), with a maximum temperature increment of 43℃. In marked contrast, the temperature of pure water does not have an obvious increase even under exposure to a high laser power density at 1.5 W/cm^2. Moreover, the photothermal stability of Au NR@PAMAM-GX1 was tested by five cycles of NIR laser irradiation (808 nm, 1.5 W/cm^2, 5 min) and cooling down (Figure 2D). Obviously, there is no obvious change in the maximum temperature value, indicating that the Au NR@PAMAM-GX1 exhibits remarkable photothermal stability and is expected to be used as PTT agents for tumor treatment.(27)

X-Ray Attenuation Property of the Au NR@PAMAM-GX1

Due to the high atomic number, gold nanoparticles have been studied as potential contrast agents for X-ray CT imaging.(28) Therefore, we measured the potential of using Au NR@PAMAM-GX1 as CT contrast agents using X-ray attenuation intensity measurements (figure 3A). We find that CT images become brighter with the increasing Au concentration. At an Au concentration of 0.04 M, the brightness of the CT image is significantly improved, which is in good agreement with the quantitative analysis of the change in X-ray attenuation intensity (also called Hounsfield unit-HU, figure 3C) of Au NR@PAMAM-GX1 as a function of Au concentration. We can surely conclude that our Au NR@PAMAM-GX1 is clinically promising as a CT imaging contrast agent, which is consistent with the previously reported literature.(29)

Formation and Characterization of Au NR@PAMAM-GX1/pDNA complexes

Because naked pDNA is easily degraded by nucleases during intracellular delivery, and negatively charged pDNA is also difficult to pass through negatively charged cell membranes, we used Au NR@PAMAM-GX1 with positive surface potential as a carrier for delivery pDNA. The gel retardation assay was performed to measure the gene compaction ability of the Au NR@PAMAM-GX1 through electrostatic interaction (figure 3B). The migration of pDNA was completely retarded by Au NR@PAMAM-GX1 with the N/P ratio of 10 or above. Therefore, to form a stable complex between pDNA and Au NR@PAMAM-GX1, an N/P ratio higher than 10 was selected. Next, the zeta potentials and sizes of the Au NR@PAMAM-

GX1/pDNA complexes with weight ratio ranging from 10:1 to 50:1. As shown in figure 3E, with the N/P ratio increases, the size of the Au NR@PAMAM-GX1/pDNA complexes gradually decreased. Zeta potential measurements show that the surface potential of all the formed complexes is reduced under each studied N/P ratio compared to the individual carriers, which is due to the charge shielding effect of negatively charged pDNA (figure 3D). When the N/P ratio is 40:1 or higher, the size and zeta potential values return to the level of Au NR@PAMAM-GX1, indicating that their stability is restored. These results indicate that Au NR@PAMAM-GX1 could become dense complexes with pDNA, and their positive charge and particle size contribute to effective endocytosis.

Cytotoxicity Assay

Before in vitro gene transfection evaluation, the cytotoxicity of Au NR@PAMAM-GX1 on HCT-8 cells and L929 cells were evaluated using CCK-8 assay over a period of 24h. Obviously, the viability of HCT-8 cells treated with Au NR@PAMAM-GX1 (Figure 6A) gradually decreased with increasing Au concentration. At the Au concentration up to 500μg/mL, the cell viability remained more than 80%, which indicates that it is pretty cytocompatibility in the given concentration range. The low cytotoxicity of Au NR@PAMAM-GX1 may result from the good biocompatibility inherent in PAMAM and the biological inertness of Au nanoparticles.

Cellular uptake of Au NR@PAMAM-GX1

The efficient absorption of cells *in vivo* is the key to achieving the biological performance of biomaterials. (30) Therefore, the uptake of Au NR@PAMAM-GX1 by HCT-8 cells was analyzed using a confocal laser scanning microscope (CLSM), in which FITC fluorescently stained Au NR@PAMAM-GX1. It was observed that the internalization of Au NR@PAMAM-GX1 was time-dependent. As the fluorescence intensity increased, it indicated that more substances were internalized under a longer incubation period (Figure 4A). Among them, Au NR@PAMAM-GX1began to enter the cell at 1h, mainly accumulating in the cytoplasm. Obviously, the cells treated with the complex for 6 hours showed a stronger green fluorescent signal than other time points, indicating that the most enriched materials in the cells were at the changed time point.

To prove the targeting ability of GX1 to HCT-8 cells, the cell uptake of Au NR@PAMAM and Au NR@PAMAM-GX1 was also compared by flow cytometry. The results are shown in Figure 4B. As expected, Au NR@PAMAM with GX1 functionalization had the strongest fluorescence intensity at the same time point, indicating that Au NR@PAMAM-GX1 absorbed by HCT-8 cells increased significantly. This indicates that GX1 does improve the delivery efficiency of the nano-system to HCT-8 cells.

In vitro gene transfection

The feasibility of Au NR@PAMAM-GX1 as gene transfection vectors was assessed by GFP gene expression experiments. Flow cytometry was used to detect the in vitro gene transfection efficiency of Au NR@PAMAM-GX1/pDNA complex with different N/P ratios in serum-containing medium, including Au NR@PAMAM-GX1/pDNA complex and PEI-25k/pDNA were set as control. We found that the transfection efficiency of the Au NR@PAMAM-GX1/pDNA complex depends on the N/P ratio (Figures 5B). It is worth noting that the gene transfection efficiency of the Au NR@PAMAM-GX1/pDNA complex with an N/P ratio of 40: 1 is the highest, with a total of 47.5% of HCT-8 cells transfected. At this time, the transfection efficiency of the Au NR@PAMAM-GX1/pDNA complex was significantly higher than that of PEI-25k/pDNA complex, and only 10.9% of cells were transfected.

In addition, we used fluorescence microscopy to detect the expression of GFP in HCT-8 cells under different complex treatments (Figure 5A). Compared with the PEI-25k/DNA complex, each N/P ratio Au NR@PAMAM-GX1/DNA complex treated HCT-8 cells had stronger fluorescence intensity, indicating that pDNA delivery efficiency of Au NR@PAMAM-GX1 is higher than PEI-25k. Among them, the number of HCT-8 cells transfected with Au NR@PAMAM-GX1/DNA complex with an N/P ratio of 40: 1 was observed to be the largest and the fluorescence intensity was the strongest. This trend is consistent with the results of flow cytometry experiments.

Combinational PTT and Gene Silencing of Cancer Cells in Vitro

The nice photothermal conversion efficiency of the Au NR@PAMAM-GX1 prompted us to use them for laser ablation of cancer cells *in vitro*. The survival rate of HCT-8 cells incubated with different Au concentrations of Au NR@PAMAM-GX1 under laser irradiation was measured by the CCK-8 method (Figure 6B). HCT-8 cells treated with AuNR@PAMAM-GX1 at different Au concentrations (10, 20, 40, 80 and 100 μg/mL) without laser irradiation did not play any obvious changes in survivability. After incubated with Au NR@PAMAM-GX1 with laser irradiation for 5 minutes, the viability of HCT-8 cells gradually decreased with the Au concentration. When the Au concentration is 80 μg/mL, almost 55.3% of cells are killed. These results indicate that AuNR@PAMAM-GX1 has an excellent tumor destruction effect.

To explore the potential of Au NR@PAMAM-GX1 polymer in combination with PTT and gene therapy cancer cells *in vitro*, the viability of HCT-8 cells was evaluated by CCK-8 assay. As shown in Figure 6C, with laser irradiation for 5 minutes, the survival rate of HCT-8 cells treated with Au NR@PAMAM-GX1 was 44.73%, while the survival rate of HCT-8 cells treated with Au NR@PAMAM-GX1/FAM172A polyplexes without laser irradiation was 57.3%. However, after cultivated with Au NR@PAMAM-GX1/FAM172A polyplexes with laser irradiation for 5 minutes, the cell survival rate dropped to 19.3%, which was significantly lower than that of single PTT and gene therapy. This highlights the effects of PTT enhancement and supercell growth inhibition after gene therapy. Fluorescence microscopy imaging of cells after different treatments further confirmed the enhancement of the treatment effect (Figure 6D). It can be seen that the number of living cells (green cells) in all control groups is Au NR@PAMAM-

GX1/FAM172A + laser < Au NR@PAMAM-GX1 + laser < Au NR@PAMAM-GX1/FAM172A < all control groups. This showed that the combination of photothermal and gene therapy was more effective in inhibiting cell proliferation.

Cell Apoptosis.

In order to further evaluate the cytotoxicity and cell death induced by gene and PTT treatment of Au NR@PAMAM-GX1 nanocomposite materials, Annexin V-FITC and PI dye staining methods were used to detect cell apoptosis. As shown in Figure 6E, in the control group, most of the cells (95.35%) were still alive. However, under light conditions, in the groups treated with Au NR@PAMAM-GX1 and Au NR@PAMAM-GX1/F172A, the proportion of viable cells decreased significantly, and the apoptosis rates were 35.43% and 43.11%, respectively. These results indicate that the genes of Au NR@PAMAM-GX1/F172A nanocomposite and apoptosis induced by the PTT effect are the main causes of cell death.

In Vivo Thermal Imaging, and Enhanced PTT and Gene Therapy of Tumors

With the excellent photothermal properties of the Au NR@PAMAM-GX1, we explored the feasibility of using it for thermal imaging of xenograft tumor models (Figure S2). The whole body thermal image of the mouse showed that during the laser irradiation, the temperature of the tumor area injected with PBS only increased by 3.2°C, while the temperature of the tumor area after the injection of Au NR@PAMAM and Au NR@PAMAM-GX1 after 300 s irradiation showed Significant temperature increases at 20.1 and 30.7°C. Compared with Au NR@PAMAM, the temperature increase of using Au NR@PAMAM-GX1 is better, which may be due to the targeting effect of GX1 polypeptide that makes more materials enrich in tumor sites.

We then measured the PTT and gene therapy effect of Au NR@PAMAM-GX1 HCT-8 tumor-bearing nude mice. The tumor suppression effects of different treatments were monitored by measuring tumor volume and tumor weight. The tumor growth curves of mice in different treatment groups were obvious within 14 days (Figure 7A). The relative tumor volume of the control group (with or without laser irradiation) and Au NR@PAMAM-GX1 without laser irradiation increased rapidly. On the contrary, the multiple clusters of Au NR@PAMAM GX1/FAM172A without laser irradiation reduced the tumor growth rate to a certain extent, which may be an independent effect of gene silencing. In addition, the treatment of Au NR@PAMAM-GX1 and Au NR@PAMAM-GX1/FAM172A multi-complex under laser irradiation significantly inhibited tumor growth. It seems that the combination of PTT and gene silencing can make tumor ablation most effective. The final size and weight of each group were measured after 14 days of tumor treatment (Figure7B and C), it clearly shows that the anti-tumor effect of the material after the order Au NR@PAMAM-GX1/ FAM172A (NIR+)> Au NR@PAMAM-GX1(NIR+)> Au NR@PAMAM-GX1/ FAM172A (NIR−)> Au NR@PAMAM-GX1(NIR−)> PBS control. There was no significant change in the body weight of the mice under different treatments at different time points, indicating that the injection of Au

NR@PAMAM-GX1 or Au NR@PAMAM-GX1/ FAM172A material, regardless of whether the laser irradiation or not, will not affect the growth state of the mouse and is not toxic to the mouse (Figure 7D).

Histologic and Immunohistochemical Analysis

The anti-tumor effect of the combined therapy Au NR@PAMAM-GX1/ FAM172A was further evaluated by histopathological analysis of HCT-8 tumor sections stained with H&E. As shown in Figure 7E, the tumor cells treated with PBS and the single light group had a complete structure and more chromatin, indicating tumor was rapid growth. The other groups treated with Au NR@PAMAM-GX1/FAM172A showed varying degrees of tumor cell nuclear shrinkage and enlarged intracellular space, suggesting that these groups showed effective treatment responses to tumors. The tumors treated by Au NR@PAMAM-GX1/ FAM172A under light conditions have the largest intracellular space and the fewest tumor cells, indicating that the combination therapy has the best effect.

The terminal deoxynucleoside transfer-induced dUTP labeling terminal labeling (TUNEL) method was used to further evaluate the effects of different treatments on apoptosis *in vivo*. Similarly, Au NR@PAMAM-GX1/FAM172A+NIR induced the highest proportion of apoptosis-positive tumor cells, confirming its strongest anticancer activity *in vivo*. Tumor sections of each group were stained with Ki67 immunohistochemical staining to monitor changes in tumor cell proliferation activity. Ki67 is a sign of cell proliferation, and light brown and blue represent the positive and negative expression of Ki67 protein, respectively. Ki67 staining results showed that Au NR@PAMAM-GX1/FAM172A+NIR treatment also significantly inhibited the proliferation activity of tumor cells.

In vivo biocompatibility evaluation

Biocompatibility is a prerequisite for the safe application of materials in nanomedicine. Therefore, we studied the *in vivo* toxicity of the Au NR@PAMAM-GX1 complex to the main organs of mice. The H&E images of the main organs of mice after 14 days of different treatments are shown in Figure 8. There is no obvious damage to the morphology and structure of the organs in each treatment group, indicating that our nanocarriers have good biological safety.

Discussion

In this study, we used gene therapy and photothermal therapy to overcome the limitations of traditional treatment methods. We have developed a new multifunctional nanocarrier AuNR@PAMAM-GX1, which has many advantages. The modified AuNR@PAMAM not only has good biocompatibility, but also maintains the LSPR phenomenon of AUNR skeleton, and has excellent photothermal conversion ability. PAMAM-modified AUNR can homing colon cancer cells via GX1 and has great potential in targeted molecular therapy of colon cancer. Relevant studies have shown that the up regulation of FAM172A gene can inhibit the proliferation, migration and invasion of colon cancer cells(31, 32). Notably,

AuNR@PAMAM-GX1/FAM172A showed excellent anti-tumor effect under the combined effect of photothermal effect and gene silencing.

Good biocompatibility is very important for the application of nanomaterials in the field of biological therapy. Cetyltrimethylammonium bromide is an essential active reagent for the synthesis of gold nanorods, although its apparent cytotoxicity limits its biological applications (33). To reduce the cytotoxicity of the material, we manipulated AUNR by externally modifying positively charged PAMAM. The results show that the modified gold nanomaterials have better biocompatibility. Even at very high concentrations (100 μg/mL) of AuNR@PAMAM-GX1, the cell survival rate remained above 80%. In addition, the small molecular size and cylindrical shape of nanorods facilitate their entry into cells through the cell membrane(34). This is particularly true of targeted therapies for cancer cells. Nanomaterial modification resulted in high accumulation of AuNR@PAMAM-GX1 in tumor cells, delivering more FAM172A to tumor cells.

Another important advantage of AUNR is that it has local surface plasmon resonance (LSPR), which can convert the absorbed light energy into heat energy under near-infrared light irradiation, thus killing and destroying cells(35). Then, we explored the photothermal conversion ability of AuNR@PAMAM-GX1, and the results show that the modified Fe can effectively induce thermal energy under the irradiation of near-infrared light. Next, we further investigated the synergistic effect of AuNR@PAMAM-GX1/FAM172A.While gene therapy has shown limited anti-tumor effects, AuNR@PAMAM-GX1 + NIR has a stronger ability to kill tumor cells. Meanwhile, the combination of photothermal hyperthermia and gene therapy showed the best antitumor effect, suggesting that the synergistic effect of AuNR@PAMAM-GX1/FAM172A and photothermal effect may be an ideal strategy for the inhibition of colon cancer.

Conclusion

In summary, we have designed an innovative combination therapy platform with PTT therapy and gene silencing capability based on dendritic molecule-stabilized Au NSs. The partially thiolated third-generation (G3) poly (amidoamine) (PAMAM) dendrimers were combined with gold nanorods to form Au NR @ PAMAM conjugate via Au-S bond. The GX1 polypeptide was combined with Au NR@PAMAM to obtain Au NR@PAMAM-GX1 through the amide reaction. Au NR@PAMAM-GX1 showed good cell compatibility within the studied concentration range and could be used as a carrier for delivering specific FAM172A to cancer cells. In addition, the Au NR@PAMAM-GX1 polyplexes can be serviced as a unique platform with enhanced PTT and gene therapy of cancer *in vitro* and *in vivo*. With the CT and thermal imaging functions of Au NR@PAMAM-GX1, it is possible to be used as an integrated diagnosis and treatment platform for cancer treatment.

Abbreviations

PTT: Photothermal Therapy; Au NRs: Gold Nanorods; SPR: Surface plasmon resonance; GT: Gene therapy; PA: Photoacoustic imaging; PAMAM: Poly (amidoamine) dendrimers; EDC: 1-ethyl-3- [3-

dimethylaminopropyl] carbodiimide hydrochloride; FTIR: Fourier transform infrared; CLSM: Confocal laser scanning microscopy; GFP: Green fluorescent protein; TUNEL: Terminal deoxynucleotidyl transferase deoxyuridine triphosphate nick-end labeling

Declarations

Acknowledgement

We sincerely appreciate all lab members.

Authors' contributions

LLY completed the synthesis and characterization of the material and wrote this manuscript, YMC completed the cell test experiment, LLY, YMC, JZM, XTL and QY jointly completed the animal experiment.

Funding

This study was supported by the National Natural Science Foundation of China (8197032867), the Science and Technology Planning Project of Guangzhou (201707010104).

Availability of data and materials

All data generated or analysed during this study are included in this published article.

Ethics approval and consent to participate

This study was approved by the ethic committee of Zhujiang Hospital Southern Medical University. Informed consent was obtained from each participant.

Consent for publication

Not applicable.

Competing interests

The authors report no conflicts of interest in this work.

Author details

1. Department of Neuro-oncological Surgery, Zhujiang Hospital, Southern Medical University, Guangzhou, Guangdong Province, China.
2. The Second School of Clinical Medicine, Southern Medical University, Guangzhou, Guangdong Province, China.

References

1. Feng W, Chen L, Qin M, Zhou X, Zhang Q, Miao Y, et al. Flower-like PEGylated MoS2 nanoflakes for near-infrared photothermal cancer therapy. Scientific Reports. 2015;5:17422.
2. Jie Yu DJ, Mohammad A. Yaseen, Nitin Nitin, Rebecca Richards-Kortum, Bahman Anvari, Wong MS. Self-assembly synthesis, tumor cell targeting, and photothermal capabilities of antibody-coated indocyanine green nanocapsules. Journal of the American Chemical Society. 2010;132(6):1929.
3. Zhang, Guixiang, Hu, Yong, Shi, Xiangyang, et al. Facile synthesis of hyaluronic acid-modified Fe3O4/Au composite nanoparticles for targeted dual mode MR/CT imaging of tumors. Journal of Materials Chemistry B Materials for Biology & Medicine. 2015;3(47):9098-9108.
4. Wen, Shihui, Tang, Yueqin, Shi, Xiangyang, et al. Construction of polydopamine-coated gold nanostars for CT imaging and enhanced photothermal therapy of tumors: an innovative theranostic strategy. Journal of Materials Chemistry B Materials for Biology & Medicine. 2016;4(23):4216-4226.
5. Wang S, Chen Y, Li X, Gao W, Zhang L, Liu J, et al. Injectable 2D MoS2-Integrated Drug Delivering Implant for Highly Efficient NIR-Triggered Synergistic Tumor Hyperthermia. Adv Mater. 2015;27(44):7117-22.
6. Mesoporous Silica Coated Single-Walled Carbon Nanotubes as a Multifunctional Light-Responsive Platform for Cancer Combination Therapy. Advanced Functional Materials. 2015;25(3):384-92.
7. Wang Y, Wang K, Zhao J, Liu X, Bu J, Yan X, et al. Multifunctional mesoporous silica-coated graphene nanosheet used for chemo-photothermal synergistic targeted therapy of glioma. Journal of the American Chemical Society. 2013;135(12):4799-804.
8. Tsai MF, Chang SHG, Cheng FY, Shanmugam V, Cheng YS, Su CH, et al. Au nanorod design as light-absorber in the first and second biological near-infrared windows for in vivo photothermal therapy. Acs Nano. 2013;7(6):5330-42.
9. Hu Y, Wang R, Wang S, Ding L, Li J, Luo Y, et al. Multifunctional Fe3O4@Au core/shell nanostars: a unique platform for multimode imaging and photothermal therapy of tumors. Scientific Reports. 2016;6:28325.
10. Luke, Henderson, Oara, Neumann, Caterina, Kaffes, et al. Routes to Potentially Safer T1 Magnetic Resonance Imaging Contrast in a Compact Plasmonic Nanoparticle with Enhanced Fluorescence. Acs Nano. 2018;12(8):8214-8223.
11. Wang C, Xu H, Liang C, Liu Y, Li Z, Yang G, et al. Iron oxide @ polypyrrole nanoparticles as a multifunctional drug carrier for remotely controlled cancer therapy with synergistic antitumor effect. Acs Nano. 2013;7(8):6782-95.

12. Vigderman L, Khanal BP, Zubarev ER. Functional Gold Nanorods: Synthesis, Self-Assembly, and Sensing Applications. Adv Mater. 2012;24(36):4811-4841.
13. Huang X, Neretina S, El-Sayed MA. Gold Nanorods: From Synthesis and Properties to Biological and Biomedical Applications. Adv Mater. 2010;21(48):4880-910.
14. Chen H, Shao L, Li Q, Wang J. Gold nanorods and their plasmonic properties. Chem Soc Rev. 2013;42(7):2679-724.
15. A QL, B TL, A MX, A LY, A YS, A NL. SO $_2$ prodrug doped nanorattles with extra-high drug payload for "collusion inside and outside" photothermal/pH triggered - gas therapy. Biomaterials. 2020;257:120236.
16. Huang Y, Liu Q, Wang Y, He N, Zhao R, Choo J, et al. Gold nanorods functionalized by a glutathione response near-infrared fluorescent probe as a promising nanoplatform for fluorescence imaging guided precision therapy. Nanoscale. 2019;11.
17. Yin F, Yang C, Wang Q, Zeng S, Hu R, Lin G, et al. A Light-Driven Therapy of Pancreatic Adenocarcinoma Using Gold Nanorods-Based Nanocarriers for Co-Delivery of Doxorubicin and siRNA. Theranostics. 2015;5(8):818-33.
18. Huanjun, Chen, Lei, Shao, Qian, Li, et al. Gold nanorods and their plasmonic properties. Chem Soc Rev. 2013;42(7):2679-2724.
19. Nie L, Wang S, Wang X, Rong P, Ma Y, Liu G, et al. In Vivo Volumetric Photoacoustic Molecular Angiography and Therapeutic Monitoring with Targeted Plasmonic Nanostars. Small. 2014;10(8):1585-93.
20. Shi S, Li D, Li Y, Feng Z, Du Y, Nie Y. LncRNA CR749391 acts as a tumor suppressor to upregulate KLF6 expression via interacting with miR-181a in gastric cancer. Experimental and Therapeutic Medicine.19(1).
21. Yan L, Zhang Y, Li K, Wang M, Zhang Y. miR-593-5p inhibit cell proliferation by targeting PLK1 in non small cell lung cancer cells. Pathology - Research and Practice. 2019:216(2):152786.
22. Wang R, Zhao N, Xu FJ. Hollow Nanostars with Photothermal Gold Caps and Their Controlled Surface Functionalization for Complementary Therapies. Advanced Functional Materials. 2017;27(23):1700256.
23. Hu Y, Zhou Y, Zhao N, Liu F, Xu FJ. Multifunctional pDNA-Conjugated Polycationic Au Nanorod-Coated Fe3O4 Hierarchical Nanocomposites for Trimodal Imaging and Combined Photothermal/Gene Therapy. Small. 2016.
24. Rae J, Jachimska B. Analysis of dendrimer-protein interactions and their implications on potential applications of dendrimers in nanomedicine. Nanoscale. 2021;13(4):2703-2713.
25. Wang S, Zhao X, Wang S, Qian J, He S. Biologically Inspired Polydopamine Capped Gold Nanorods for Drug Delivery and Light-Mediated Cancer Therapy. ACS Applied Materials & Interfaces. 2016;8(37):24368-24384.

26. Pan B, Gao F, Ao L, Tian H, He R, Cui D. Controlled self-assembly of thiol-terminated poly(amidoamine) dendrimer and gold nanoparticles. Colloids & Surfaces A Physicochemical & Engineering Aspects. 2005;259(1-3):89-94.
27. Terentyuk GS, Ivanov AV, Polyanskaya NI, Maksimova IL, Skaptsov AA, Chumakov DS, et al. Photothermal effects induced by laser heating of gold nanorods in suspensions and inoculated tumours during in vivo experiments. Quantum Electronics. 2012;42(5):380-389.
28. Bian L, Li HL, Li YJ, Nie JN, Xie L. Enhanced Photovoltage Response of Hematite-X-Ferrite Interfaces (X = Cr, Mn, Co, or Ni). Nanoscale Res Lett. 2017;12(1):136.
29. Wei P, Chen J, Hu Y, Li X, Wang H, Shen M, et al. Dendrimer-Stabilized Gold Nanostars as a Multifunctional Theranostic Nanoplatform for CT Imaging, Photothermal Therapy, and Gene Silencing of Tumors. Advanced Healthcare Materials. 2016;5(24):3203-3213.
30. Gonzalez-Moragas L, Berto P, Vilches C, Quidant R, Kolovou A, Santarella-Mellwig R, et al. In vivo testing of gold nanoparticles using the Caenorhabditis elegans model organism. Acta Biomater. 2017;53:598-609.
31. Cui C, Ye L, Huang Z, Huang S, Liu H, Yu J. FAM172A is a tumor suppressor in colorectal carcinoma. Tumor Biology. 2015;37(5):6501-6510.
32. Bélanger C, Bérubé-Simard F-A, Leduc E, Bernas G, Campeau PM, Lalani SR, et al. Dysregulation of cotranscriptional alternative splicing underlies CHARGE syndrome. Proceedings of the National Academy of Sciences of the United States of America. 2018;115(4):E620-E629.
33. Sun Q, Shi X, Feng J, Zhang Q, Han D. Cytotoxicity and Cellular Responses of Gold Nanorods to Smooth Muscle Cells Dependent on Surface Chemistry Coupled Action. Small. 2018;14(52):1803715.
34. Hope, Michael, J., Cullis, Pieter, R. Lipid Nanoparticle Systems for Enabling Gene Therapies. Molecular Therapy the Journal of the American Society of Gene Therapy. 2017;25(7):1467-1475.
35. Zhang C, Cheng X, Chen M, Sheng J, Ren J, Jiang Z, et al. Fluorescence guided photothermal/photodynamic ablation of tumours using pH-responsive chlorin e6-conjugated gold nanorods. Colloids Surf B Biointerfaces. 2017;160:345-354.

Figures

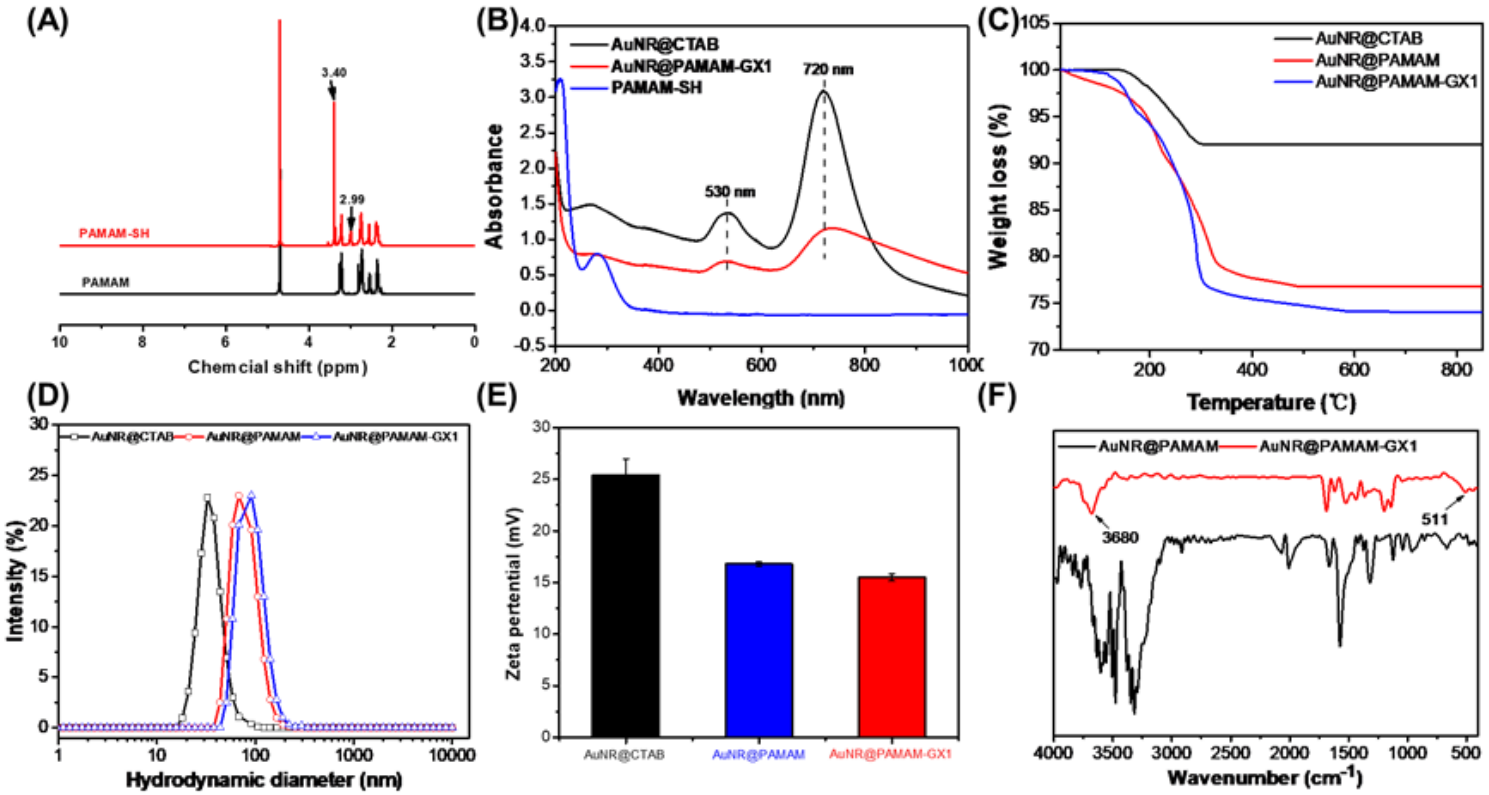

Figure 1

Characterizations of AuNR@PAMAM-GX1. (A) 1H NMR spectra for PAMAM and PAMAM-SH. (B) UV-Vis spectra of Au NR@CTAB, AuNR@PAMAM and PAMAM-SH. (C) TG curves of Au NR@CTAB, Au NR@PAMAM and Au NR@PAMAM-GX1. (D) hydrodynamic diameter of Au NR@CTAB, Au NR@PAMAM and Au NR@PAMAM-GX1. (E) zeta potential of Au NR@CTAB, Au NR@PAMAM and Au NR@PAMAM-GX1. (F) FTIR spectra of Au NR@PAMAM and Au NR@PAMAM-GX1.

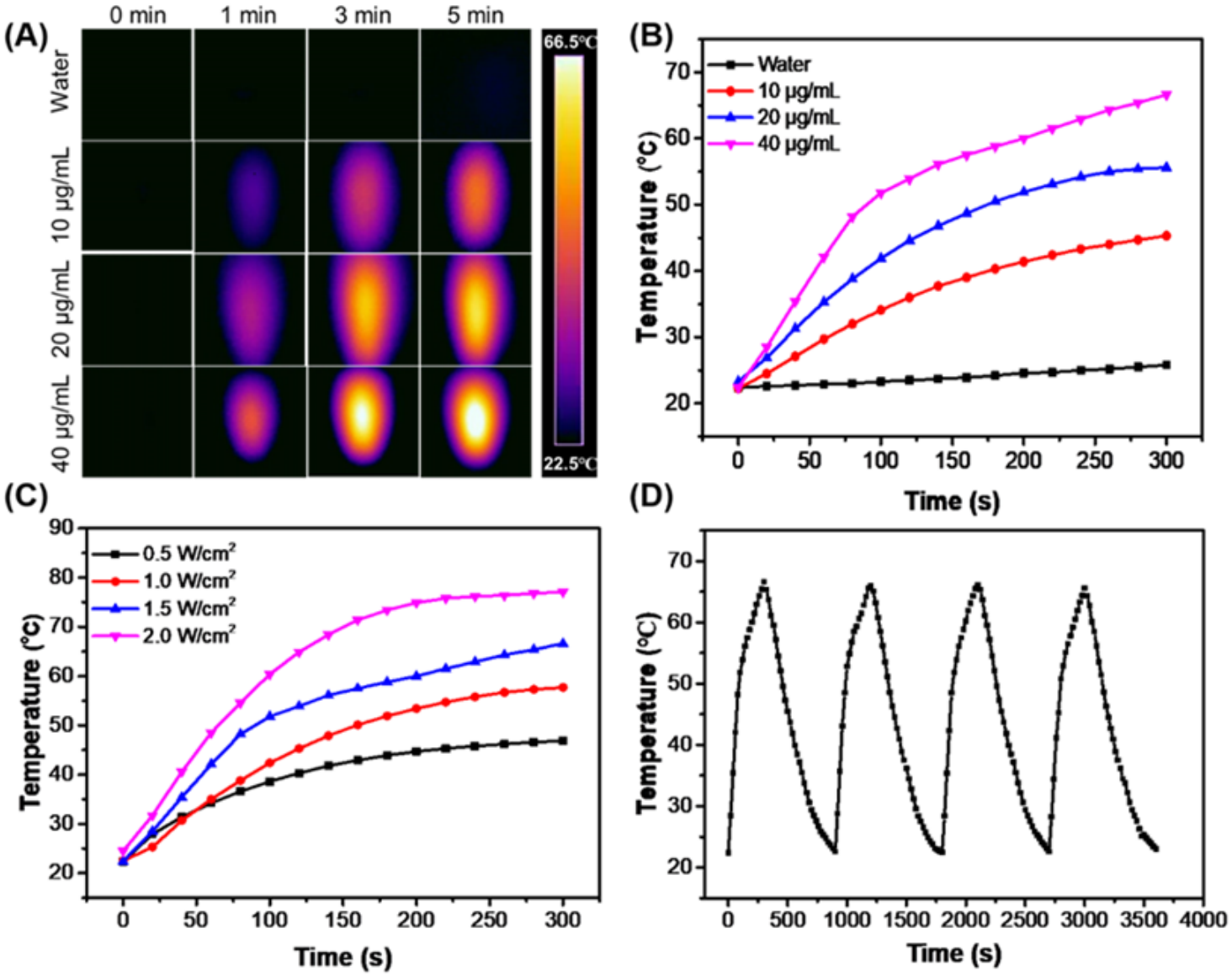

Figure 2

(A) Infrared thermal images and (B) temperature of the solution containing Au NR@PAMAM-GX1 under the NIR laser (808 nm, 1.5 W/cm2) irradiation for 5 min. (C) Temperature of the solution containing Au NR@PAMAM -GX1 at different laser power density. (D) Temperature of the solution containing Au NR@PAMAM-GX1 (40 μg/mL) under laser ON/OFF cycles of NIR laser (1.5 W/cm2) irradiation.

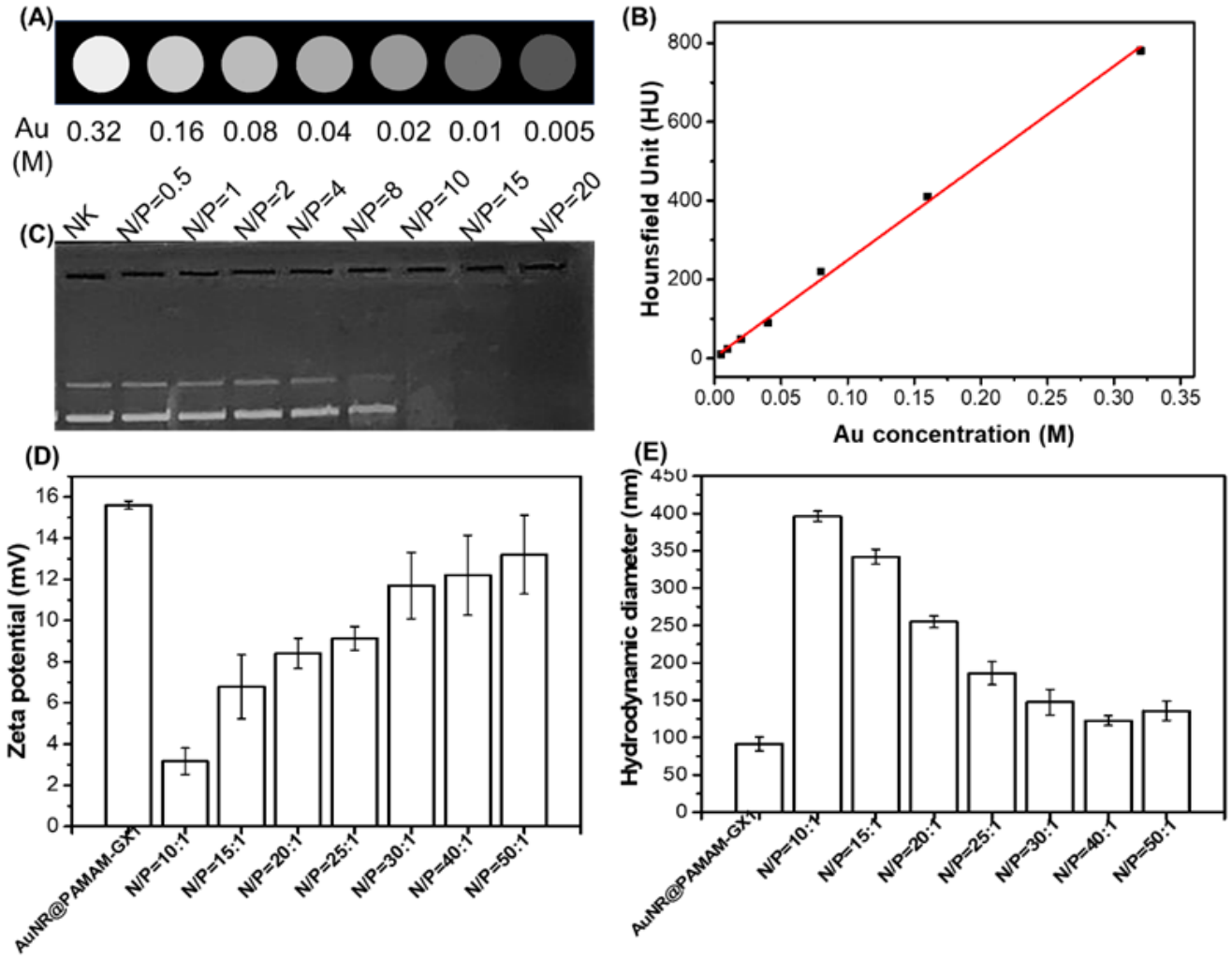

Figure 3

Characterization of Au NR@PAMAM-GX1 and Au NR@PAMAM-GX1 /pDNA complexes. CT images (A) and X-ray attenuation intensity (B) of Au NR@PAMAM-GX1 with different concentrations. (C) Gel retardation assay of Au NR@PAMAM-GX1/pDNA with different N/P ratios. (D) Zeta potential and (E) hydrodynamic diameter of Au NR@PAMAM-GX1/pDNA with different N/P ratios.

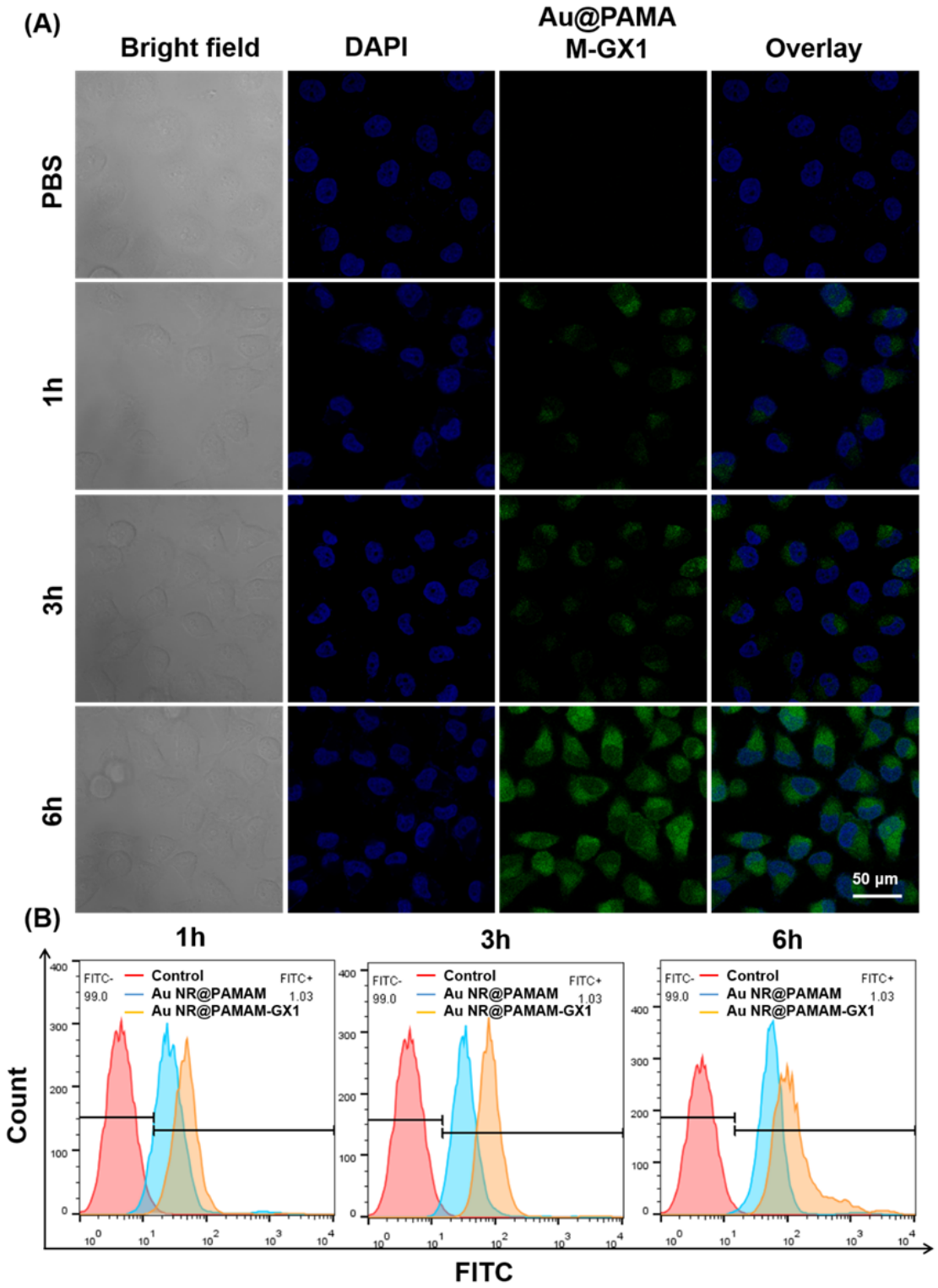

Figure 4

(A) Cellular uptake evaluation of Au NR@PAMAM-GX1 using CLSM over an incubation period of 6h, where nuclei were stained by DAPI displaying blue fluorescence, Au NR@PAMAM-GX1 were FITC labeled showing green fluorescence. (B) Flow cytometry analysis of fluorescence peak figure in HCT-8 cells incubated with Au NR@PAMAM or Au NR@PAMAM-GX for different time.

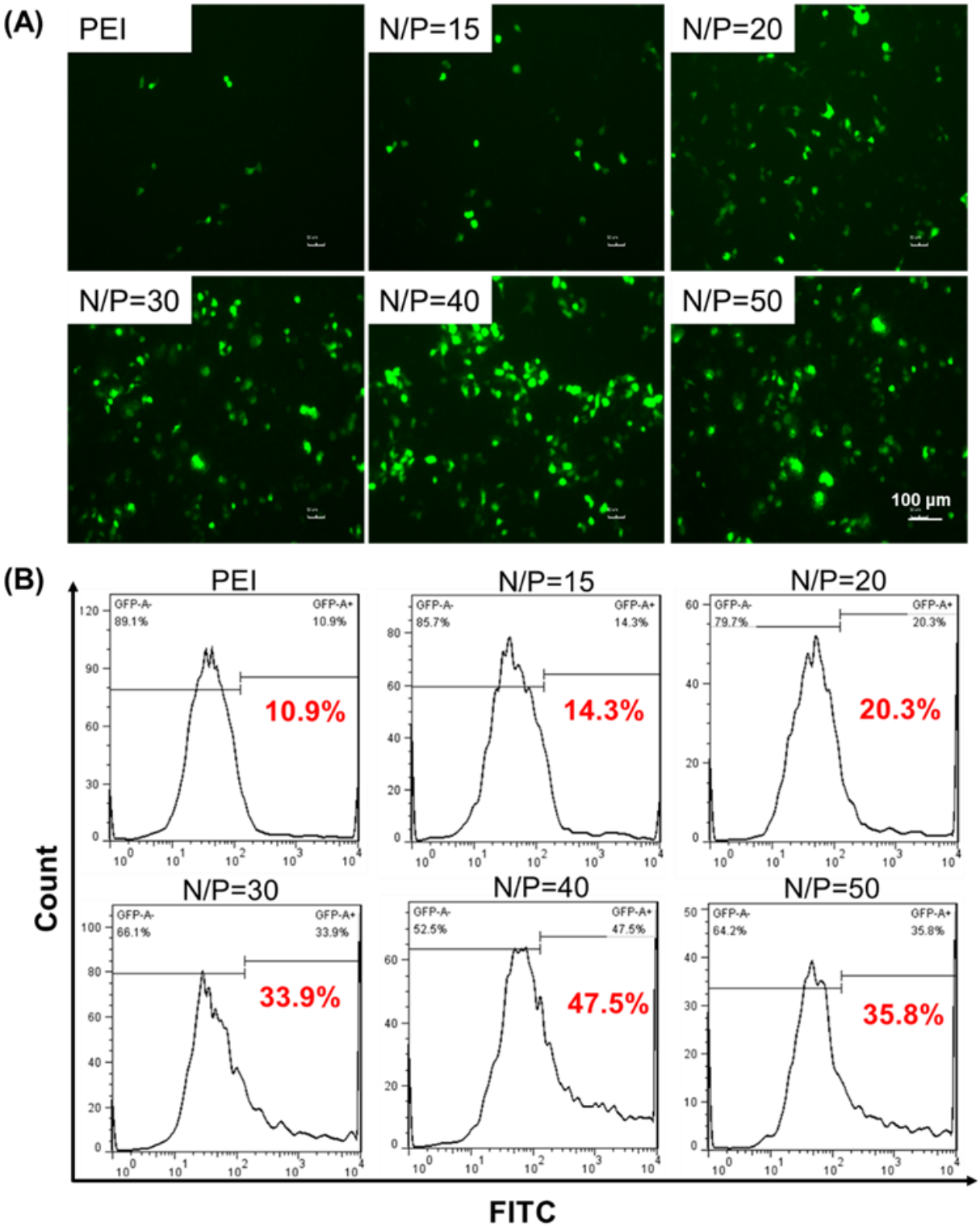

Figure 5

In vitro gene transfection efficiency evaluation of Au NR@PAMAM-GX1/pDNA complexes. (A) In the presence of serum, fluorescence images of HCT-8 cells transfected with Au NR@PAMAM-GX1/pDNA complexes in different weight ratios. (B) The gene transfection efficiency of Au NR@PAMAM-GX1/pDNA with different N/P ratios were determined using flow cytometry.

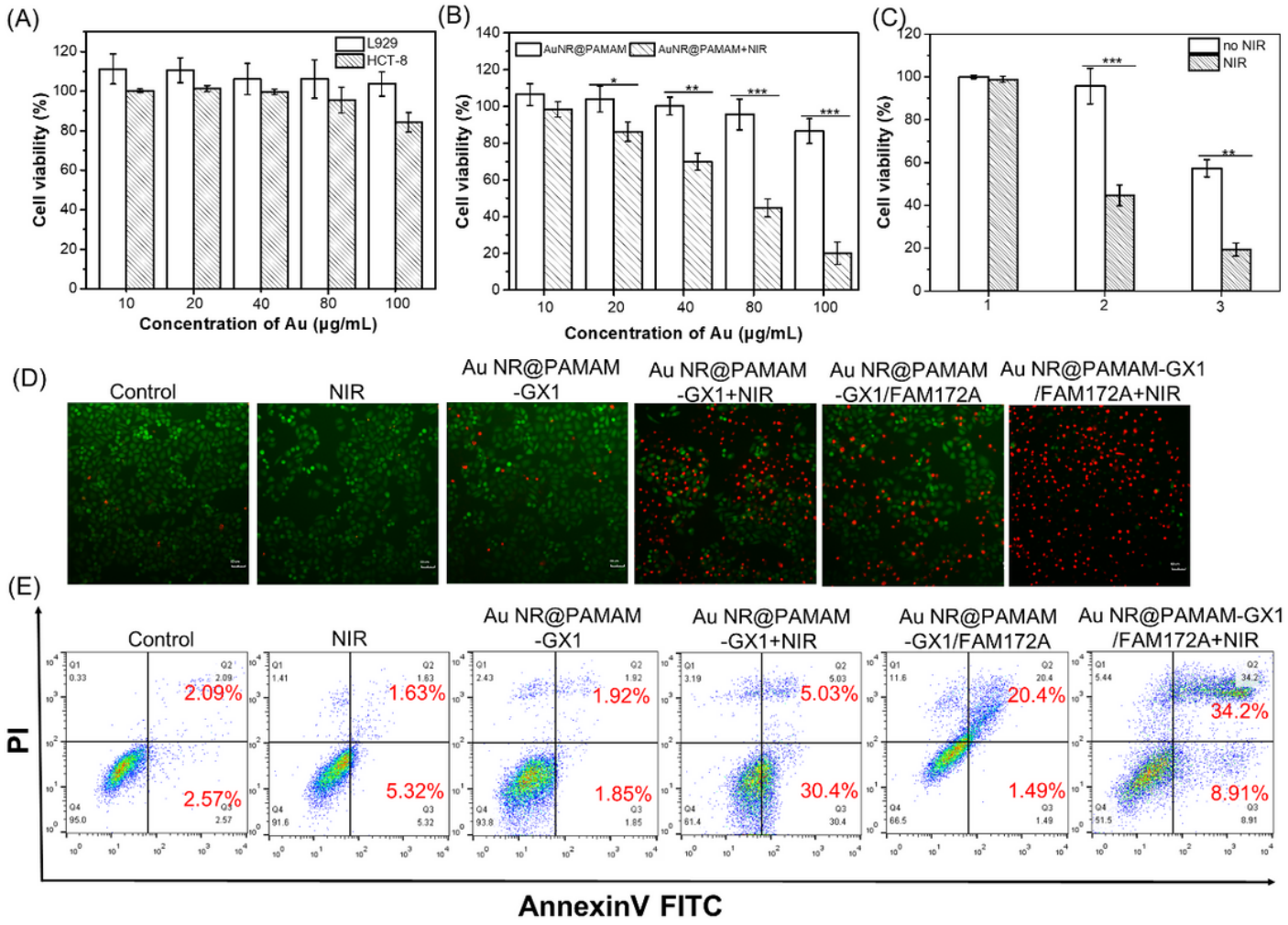

Figure 6

(A) In vitro cytotoxicity of Au NR@PAMAM-GX1/pDNA with different N/P ratios on HCT-8 cells and L929 cells over an evaluation period of 24h. (B) Cell viability of HCT-8 cells pretreated by Au NR@PAMAM-GX1 with different concentrations with and without NIR irradiation. (C) CCK-8 assay of HCT-8 cells viability after treatment with the Au NR@PAMAM-GX1or Au NR@PAMAM -GX1/FAM172A polyplexes (N/P = 40:1, 1 μg FAM172A per well) for 24 h, followed by laser irradiation for 5 min (1: PBS; 2: Au NR@PAMAM-GX1; 3: Au NR@PAMAM-GX1/FAM172A). (D) Images of PI and Calcein-AM double-stained HCT-8 cells under different treatments. (E) Flow cytometry analysis of HCT-8 cell apoptosis in different treatment groups.

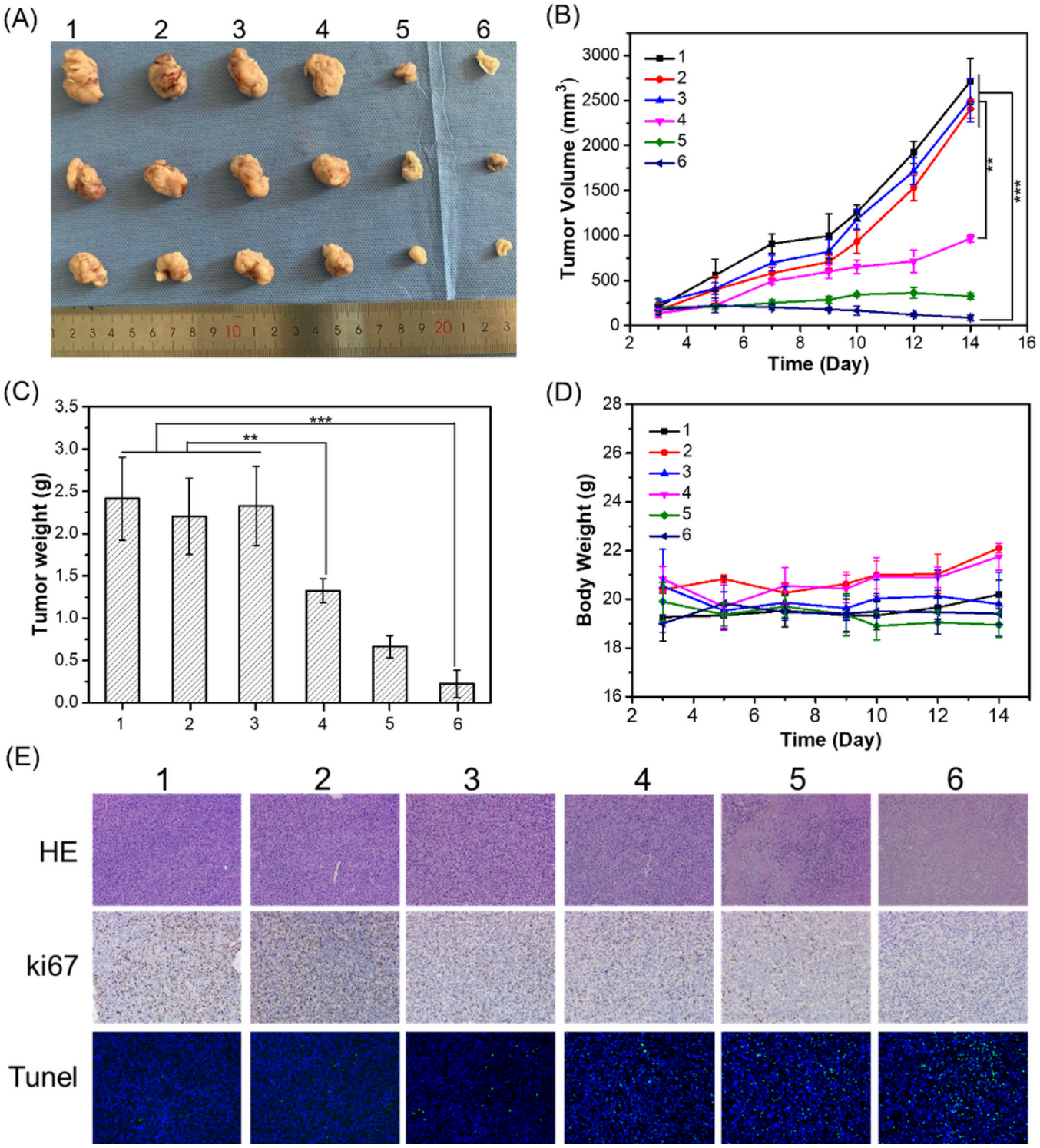

Figure 7

(A) In vivo tumor growth curves of HCT-8 tumor-bearing mice treated with different formulations. (B) Representative image of HCT-8 tumors at the 14st day. (C) The tumor weights excised from different groups after 14 days treatment. (D) Body weight changes of mice treated with different formulations during the treatment. (E) Immunohistochemical analyses of H&E, TUNEL, CD31 and Ki67 for HCT-8 tumor tissues after the last treatment with different formulations in vivo (200×) (1: PBS; 2: PBS+NIR; 3: Au

NR@PAMAM-GX1; 4: Au NR@PAMAM-GX1 / FAM172A; 5: Au NR@PAMAM-GX1+NIR; 6: Au NR@PAMAM-GX1/FAM172A +NIR).

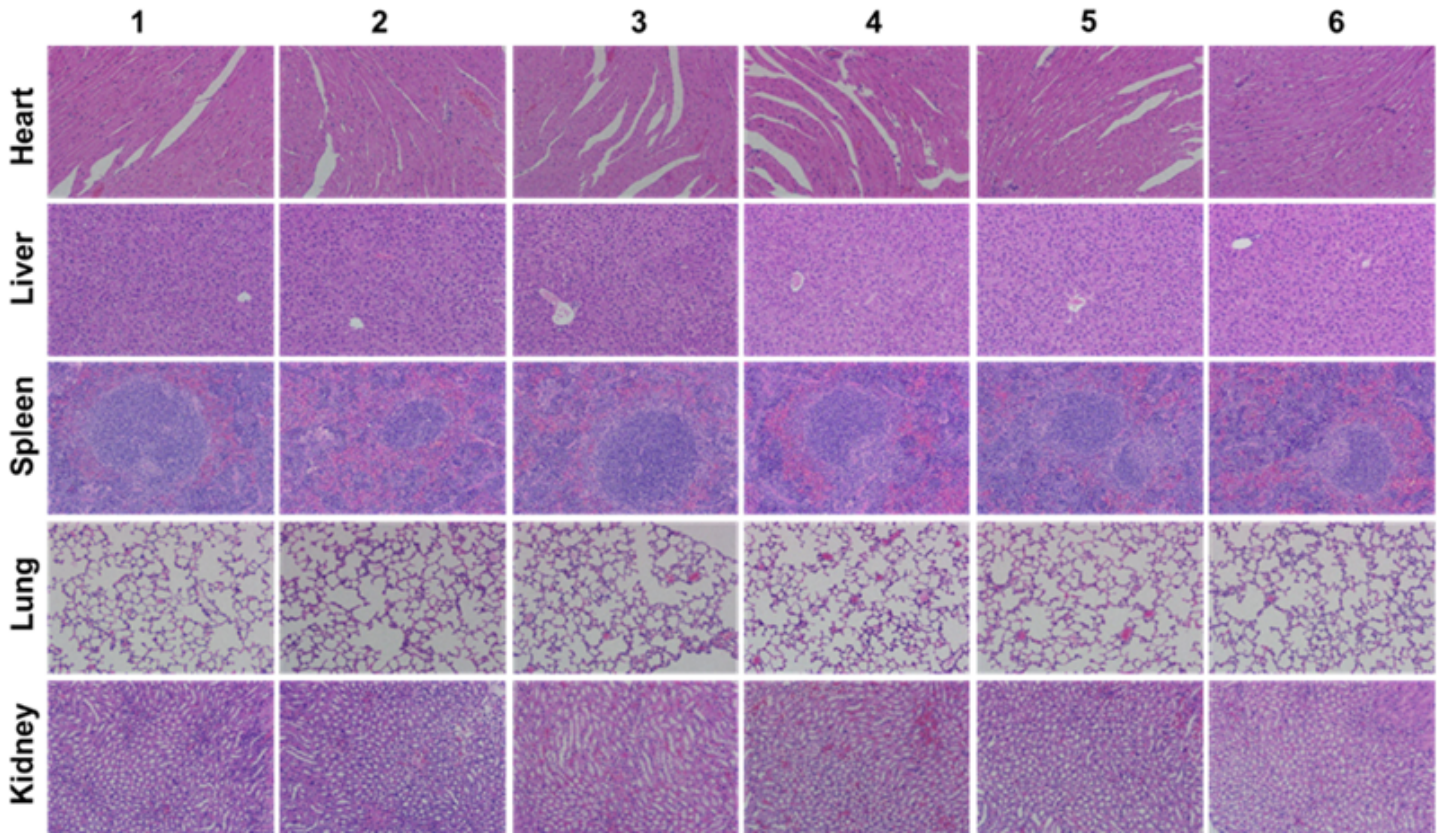

Figure 8

Histologic assessments of major organs in mice (200×) treated with different formulations. (1: PBS; 2: PBS+NIR; 3: Au NR@PAMAM-GX1; 4: Au NR@PAMAM-GX1/FAM172A; 5: Au NR@PAMAM -GX1+NIR; 6: Au NR@PAMAM-GX1/FAM172A +NIR).

Supplementary Files

This is a list of supplementary files associated with this preprint. Click to download.

- S1.jpeg
- S2.png